

THEORETICAL AND LABORATORY STUDIES ON THE INTERACTION OF COSMIC-RAY PARTICLES WITH INTERSTELLAR ICES. I. SYNTHESIS OF POLYCYCLIC AROMATIC HYDROCARBONS BY A COSMIC-RAY-INDUCED MULTICENTER MECHANISM

R. I. KAISER¹ AND K. ROESSLER²

Received 1995 December 29; accepted 1996 August 5

ABSTRACT

Methane, ethylene, and acetylene ices were irradiated in a ultra-high vacuum vessel between 10 K and 50 K with 7.3 MeV protons as well as 9.0 MeV He²⁺ nuclei to simulate the interaction of galactic cosmic-ray particles with extraterrestrial, organic ices and to elucidate a mechanistic model to synthesize experimentally detected polycyclic aromatic hydrocarbons (PAHs). Theoretical calculations center on computer simulations of ion-induced collision cascades in irradiated methane targets. MeV ions induce hydrogen and carbon knock-on particles in elastic encounters with the target atoms. Each primary knock-on triggers one collision cascade with up to 70 suprathreshold carbon atoms concentrated in one to two subcascades in $0.6\text{--}5 \times 10^3 \text{ \AA}^3$. At the end point of each single trajectory, every suprathreshold carbon atom can form an individual reaction center of hydrogen abstraction and insertion in or addition to chemical bonds of a reactant molecule. In the relaxation phase of this energized volume, overlapping reaction zones likely form observed PAHs naphthalene, phenanthrene/azulene, and coronene. This multicenter mechanism establishes a versatile route to synthesize complex molecules in extraterrestrial ices even at temperatures as low as 10 K within cosmic-ray-initiated single collision cascades.

Subject headings: cosmic rays — ISM: molecules — molecular processes

1. INTRODUCTION

Polycyclic aromatic hydrocarbons (PAHs) and their derivatives, i.e., cations, anions, radicals, alkyl- and oxygen-substituted PAHs, as well as partially hydrogenated PAHs, are among the most fascinating molecules supposed to exist in the interstellar medium (ISM) (Allamandola, Sandford, & Wopenka 1987; Geballe et al. 1989; Allamandola 1990; Schutte et al. 1990; Salama & Allamandola 1991, 1992; Schutte, Tielens, & Allamandola 1993; Salama, Joblin, & Allamandola 1994; Snow et al. 1995; Millar et al. 1995; Ehrenfreud et al. 1995; Allain, Leach, & Sedlmayr 1996a, 1996b). The very first postulation of their interstellar relevance as the missing link between small carbon clusters C₂ to C₅ and amorphous carbon particles (Leger & Puget 1984) fueled enormous scientific research. Currently, PAH-like molecules are presumed to tie up 10%–20% of the cosmic carbon and are regarded as a potential carrier of unidentified infrared bands (UIRs) at 3030, 2915, 2832, 1612, 1300, 1150, and 885 cm⁻¹ (Bergman et al. 1994; Salama & Allamandola 1992; Duley 1994; Joblin et al. 1994; Siebenmorgen & Peletier 1994; Encrenaz, d'Hendecourt, & Puget 1988; Allamandola, Tielens, & Barker 1985; Jochims et al. 1994; Pauzat, Talbi, & Ellinger 1995; Joblin et al. 1995, 1996; Langhoff 1996). Similarly, PAH species might contribute to the family of diffuse, interstellar absorption bands (DIBs) covering the visible spectrum from 440 nm to the near-infrared (Jochims et al. 1994; Ehrenfreud et al. 1995) and are thought to generate IR emission features in the spectrum of comet P/Halley (Encrenaz, d'Hendecourt, & Puget 1988).

Despite their potential crucial contribution to the cosmic carbon budget, theoretically and experimentally well-defined mechanisms to synthesize PAHs in extraterrestrial environments have not yet been elucidated. Stein (1978) proposed a stepwise association of molecules containing two and four carbon atoms via benzene in carbon-rich outflows as a potential reaction pathway in the gas phase, whereas Frenklach & Feigelson (1989) assume equilibrium rate polymerization of acetylene in circumstellar envelopes. The identification of naphthalene, alkylnaphthalenes, phenanthrene, and nitrogen-substituted PAHs in the Murchison C2 chondrite (Bakes & Tielens 1994; Hayatsu et al. 1979, Mullie & Risse 1987), however, suggests a potential influence of solid-state chemistry. Since the ISM is interspersed with high energetic galactic cosmic-ray particles, interstellar ices undergo chemical processing, and PAHs might be produced.

These results ignited our research to extract a novel model based on laboratory and theoretical studies on the interaction of cosmic-ray particles with the simplest alkane, CH₄ (methane), alkene, C₂H₄ (ethylene), and alkyne, C₂H₂ (acetylene) in interstellar ices at temperatures between 10 and 50 K. The prime directive of our experiments is to focus on *deliberate model compounds* and establish a *mechanistic model* before extending studies to astrophysical relevant systems. The choice of MeV particles in our experiments characterizes the flux distribution maximum of galactic cosmic-ray particles consisting of ~97% protons and 3% helium nuclei; radiation doses represent equivalent irradiation by the interstellar cosmic-ray particle field of $\approx 1 \times 10^9$ yr.

The reaction mechanism to PAHs is elucidated by (a) variation of the energy transfer from the implanted ion to the methane target, the so-called averaged linear energy transfer (LET) from $4.0 \pm 0.2 \text{ keV } \mu\text{m}^{-1}$ (7.3 MeV protons; hereafter system 1) to $45 \pm 5 \text{ keV } \mu\text{m}^{-1}$ (9 MeV α -particles; hereafter system 2), (b) increasing the absorbed energy per

¹ Institut für Nuklearchemie, Forschungszentrum Jülich, 52425 Jülich, Germany. Present address: Department of Chemistry, University of California, Berkeley, CA 94720; kaiser@leea.cchem.berkeley.edu.

² Institut für Nuklearchemie, Forschungszentrum Jülich, 52425 Jülich, Germany.

target molecule, dose D , up to 30 ± 3 eV, (c) probing reactions of high-energy (1–10 eV), suprathreshold atoms triggered by knock-on particles in the collision cascades, (d) analyzing thermally induced chemistry such as diffusion of H atoms, CH, CH₂, and CH₃ radicals via substitution of CH₄ by CD₄, varying the temperature during the irradiation from 10 K to 50 K, and addition of O₂ as a radical scavenger, and (e) reducing the C/H ratio of the frosts from 1:4 (CH₄) over 1:2 (C₂H₄) to 1:1 (C₂H₂). CH₄/CD₄ mixtures were probed to distinguish between inter- and intramolecular reactions and rearrangements, whereas ¹³CH₄ targets were chosen to verify on-line and in situ Fourier transform infrared (FTIR) spectroscopy and quadrupole mass spectrometry (QMS) data.

This paper is laid out as follows: § 2 focuses on the experimental setup and data acquisition, whereas § 3 describes the computer simulation routine to extract detailed collision cascades and energy transfers by protons and α -particles as well as carbon atoms to CH₄ frosts. Actual physical conditions during the PAH synthesis—successive collisions of the high-energy particle with individual target atoms and a hydrogen atom limited radical diffusion—are presented in § 4 together with PAH detection via FTIR/QMS. A model leading to PAHs by interaction of cosmic-ray particles with frozen hydrocarbons within single collision cascades and astrophysical implications are discussed in §§ 5 and 6, respectively.

2. EXPERIMENTAL APPROACH

The experimental setup was described earlier in detail (Kaiser, Gabrysch, & Roessler 1995a). The simulation experiments were performed in an ultra-high vacuum (UHV) chamber equipped with a closed cycle helium refrigerator and an attached silver wafer. Ice layers are prepared by depositing gases on a cooled wafer, keeping the cold finger at 10 K for 60 minutes, heating the ices to 35 K with 0.005 K s^{-1} , equilibrating at 35 K for 1 hr, and cooling down to 10 K with 0.005 K s^{-1} ; see Table 1. Since a constant LET is crucial to guarantee target depth-invariant reaction mechanisms, the target thickness is limited to $5 \pm 1 \mu\text{m}$, well below the range of 7.3 MeV protons and 9 MeV α particles with $926 \pm 2 \mu\text{m}$ and $128 \pm 8 \mu\text{m}$. Hydrocarbon-free UHV conditions of about 4×10^{-10} mbar are supplied by a membrane, molecular drag, and cryopump proved to be essential to exclude organic contamination and restrict condensation of residual gases onto the silver wafer to one monolayer in ≈ 10 hr. Ion fluxes ϕ of 9.0 MeV He²⁺ and 7.3

MeV H⁺ were adjusted to $\phi(\alpha) = 127 \text{ nA cm}^{-2}$ and $\phi(p) = 111 \text{ nA cm}^{-2}$ to limit the temperature increase of the frost surface to 4 ± 1 K. All targets are irradiated isothermally at 10 K or during the temperature program 10 K–50 K (ion beam on; target 6 minutes at 10 K, heating to 50 K in 20 minutes with 2 K per minute; 34 minutes at 50 K; beam off; cooling in 1 minute to 10 K). Hereafter, each 10 K irradiation is designated as “low temperature” (LT), whereas experiments during heating the sample to 50 K are defined as “high temperature” (HT). Gases are supplied by MSD Isotopes [¹³CH₄ (99.9% ¹³C); CD₄ (99.9% D); ¹²CH₄ (99.9% ¹²C)], and Messer Griesheim [O₂ (99.998%); C₂H₂ (99.6%); C₂H₄ (99.95%)] and are used without further purification. Blank checks via QMS and FTIR showed no PAH contaminations.

The solid state is monitored on line and in situ with a Fourier transform infrared (FTIR) spectrometer (4000–400 cm⁻¹; NICOLET) in absorption-reflection, whereas a calibrated quadrupole mass spectrometer (QMS) probes the gas phase. Data processing is performed via matrix interval algebra (Kaiser et al. 1995b). Briefly, m/e ratios are chosen to result in an inhomogeneous system of linear equations including the measured ion current (right-hand vector), partial pressures (unknown quantity), and calibration factors of fragments of individual gaseous species determined in separate experiments. Since all quantities are provided with experimental errors, matrix interval arithmetic, i.e., an IBM high-accuracy arithmetic subroutine defining experimental uncertainties as intervals, is incorporated in the computations to extract individual, calibrated components of gas mixtures.

3. COMPUTER SIMULATION MODEL

Physical processes triggered by the ion implantation into the CH₄ target were simulated with the MARLOWE code (Robinson 1992; Roessler 1992). This program calculates elastic and inelastic energy transfers from an impinging high-energy particle to the target atoms of the condensed hydrocarbon ices. The elastic energy loss of a binary collision between the projectile and the target atoms initiates the energetic knock-on particle and is treated by a repulsive Thomas-Fermi-Molière central potential (Molière 1947), whereas the nonrelativistic, inelastic energy loss leading to ionization and excitation is calculated via an empirically modified Firsov model atom (Firsov 1957, 1962). Since the original MARLOWE code justifies only simulations with projectile kinetic energies up to 0.1 MeV, quantum me-

TABLE 1
COMPILATION OF IRRADIATION EXPERIMENTS AND PARAMETERS

Target	Temperature	Layer Thickness (μm)	Ion	Pressure (10^{-10} mbar)	Wafer Temperature (K)	Irradiation Time (minutes)	Dose (eV)
¹³ CH ₄	LT	4.0 ± 0.4	α	4.8 ± 0.8	9.9 ± 0.2	60	29 ± 3
¹³ CH ₄	HT	4.1 ± 0.4	α	5.2 ± 0.9	10.4 ± 0.4	60	30 ± 5
CD ₄	LT	5.5 ± 1.5	α	4.8 ± 0.4	9.8 ± 0.1	60	30 ± 4
CD ₄	HT	6.5 ± 0.9	α	2.8 ± 0.3	9.7 ± 0.1	60	29 ± 4
CH ₄	LT	4.3 ± 0.5	α	3.3 ± 0.3	9.1 ± 0.1	60	29 ± 2
CH ₄	LT	4.0 ± 0.4	p	3.7 ± 0.4	9.6 ± 0.1	336	28 ± 3
C ₂ H ₄	LT	2.5 ± 0.3	α	5.2 ± 0.5	9.3 ± 0.1	78	28 ± 2
C ₂ H ₂	LT	3.0 ± 0.1	α	4.2 ± 0.4	9.8 ± 0.1	90	27 ± 2
CH ₄ /O ₂ (1%–2% O ₂).....	LT	6.9 ± 0.7	α	5.5 ± 1.0	11.0 ± 0.5	60	28 ± 5
CH ₄ /O ₂ (1%–2% O ₂).....	HT	4.8 ± 0.6	α	5.1 ± 1.2	10.8 ± 0.1	60	28 ± 5

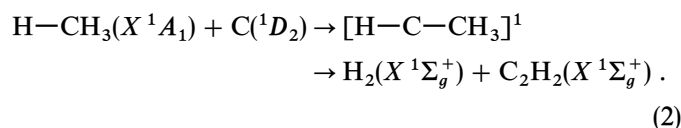
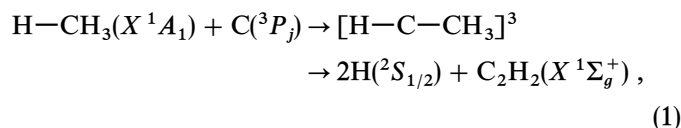
chanical and relativistic extensions are included using the Bethe-Bloch equation to account for our MeV particles (Eckstein 1991).

4. RESULTS

4.1. Irradiation Experiments

4.1.1. Thermal Equilibrium versus Single Encounters

The interpretation of ion bombardments depends strongly on the imposed physical model. Model 1 implies local thermal equilibrium and assumes generation of plasma-like conditions together with a local target melting in the interaction region. Alternatively, successive collisions of the suprathreshold particle with individual target atoms are discussed (model 2). In our experiments, the actual physical conditions are elucidated by probing acetylene molecules during LT 9 MeV α -particle irradiation of a mixed CH_4/CD_4 target via FTIR and QMS. The mechanism to acetylene formation is well established in ^{11}C hot atom tracer studies and proceeds by insertion of one carbon atom into the C—H bond of a single methane molecule via an internally excited methylcarbene (Stöcklin 1969):



If model 1 held, the relaxation phase of the plasma would go hand in hand with statistical bond formation of C, H, and D atoms to C_2H_2 , C_2D_2 , as well as C_2HD . Single encounters in model 2, however, should synthesize C_2H_2 and C_2D_2 entirely; see equations (1) and (2). Since only IR absorptions of C_2H_2 at ν_3 (3269–3209 cm^{-1}), ν_5 (809–729 cm^{-1}), and ν_2 (1990–1960 cm^{-1}) (Pearl 1994), and C_2D_2 at ν_3 (2433–2368 cm^{-1}) and ν_5 (548–539 cm^{-1}) (Smit, van Straten, & Visser 1978) were monitored, plasma-like conditions (model 1) can be dismissed. These findings gain support from QMS data showing only signal at $m/e = 26$ (C_2H_2) and $m/e = 30$ (C_2D_2), but no $m/e = 27$ (C_2HD) within the 1 amol (10^5 molecules) detection limit of our system.

4.1.2. Target Temperature and Radical Mobility

The target temperature can influence any reaction mechanism dramatically. Diffusion of H and D atoms in

solid CH_4 onsets at temperatures $T > 11$ – 12 K (Trakhtenberg & Milikh 1983). The surface temperature of condensed CH_4 layers rises during the ion bombardments from 10 K to 14 ± 1 K, whereas the temperature of the silver waver is constant at 10 ± 0.5 K (Kaiser et al. 1995a).

The mobility of H and D atoms in our experiments is well documented by formation of CHD_3 molecules via recombination of CH_3 and D and a QMS signal at $m/e = 3$ originating in H and D recombination to HD during the 9 MeV α -particle irradiation of CH_4/CD_4 targets. Further, FTIR spectra of LT experiments with CH_4/O_2 samples identify absorption features of hydrogenperoxy radicals (HO_2 ; $\nu_2 = 1409$ – 1395.5 cm^{-1} [Hagen 1987]) as a reaction product of H atoms with nonmobile, matrix isolated O_2 . No molecular hydrogen release was probed either in the irradiation phase or during heating to 293 K within the experimental error limits for C_2H_4 , C_2H_2 , and $^{12}\text{CH}_4/\text{O}_2$ targets. Comparisons of LT with HT irradiation of $^{12}\text{CH}_4$ and CD_4 depict an increasing number of hydrogen molecules released in the actual irradiation phase as the temperature rises, $[\text{H}_2(\text{HT})/\text{H}_2(\text{LT})] = 21 \pm 9$ and $[\text{D}_2(\text{HT})/\text{D}_2(\text{LT})] = 46 \pm 41$.

Finally, the mobility of larger radicals CH_2 , CD_2 , CH_3 , and CD_3 starts between 60 and 75 K, well below the temperature in LT experiments of $T < 15$ K. In a strong coincidence, no isotopically mixed recombination products $\text{C}_2\text{H}_2\text{D}_2$ ($\text{CH}_2 + \text{CD}_2$) and $\text{C}_2\text{H}_3\text{D}_3$ ($\text{CH}_3 + \text{CD}_3$) were detected either via QMS or FTIR.

4.1.3. Aromatic Species

4.1.3.1. Fourier Transform Infrared Spectroscopy

Proton-irradiated $^{12}\text{CH}_4$ targets (LT) show typical IR absorptions of aromatic vibration modes. These include the C—H stretching at 3019 cm^{-1} , ring vibrations of mono, ortho, meta, para, 1.2.4, and 1.3.5 substituted benzenes at 1607, 1593, and 1581 cm^{-1} , and the corresponding out-of-plane δ_{op} (870, 867 cm^{-1} : one isolated hydrogen atom; 855, 842 cm^{-1} : two isolated hydrogen atoms), and in-plane δ_{ip} (1110, 1086, 1073, 1066, 1053, 1044, 1039, 1026, 1039, 1026, 993, 975, and 970 cm^{-1} : para and 1.2.4. substituted benzenes) deformation modes; see Table 2. The 9 MeV LT α -particle irradiation of $^{12}\text{CH}_4$ produced identical aromatic patterns, but absorptions of 1.4 and 1.2.4 substituted benzenes at 1073, 1065, 1052.7, 1044, 1026, 1017, and 898 cm^{-1} , as well as features of three neighboring aromatic H atoms at 804 cm^{-1} , increase by a factor of ≈ 2 . Experiments with $^{13}\text{CH}_4$ stress these assignments and show aromatic absorption pattern at 3034 cm^{-1} (^{13}C —H—stretching vibration; aromatic hydrogen) and deformation modes of substituted

TABLE 2
IR ABSORPTION FEATURES OF AROMATIC SPECIES AND ASSIGNMENTS AFTER 7.3 MeV PROTON
AND 9 MeV α -PARTICLE IRRADIATION OF CH_4 AT 10 K

Absorption (cm^{-1})	Assignment
3019	Aromatic CH-stretching vibration
1607, 1593, 1581	Ring vibrations of mono, ortho, meta, para, 1.2.4, and 1.3.5 substituted benzenes
870, 867	Out-of-plane vibration of benzenes with one isolated H atom
855, 842	Out-of-plane deformation of benzenes with two isolated H atoms
1110, 1086, 1073, ^a 1066, ^a 1053, ^a 1044, ^a 1039, 1026, ^a 993, 975, 970, 804	In-plane deformation of para and 1.2.4. substituted benzenes

^a An absorption that dominates 9 MeV α -particle irradiation experiments.

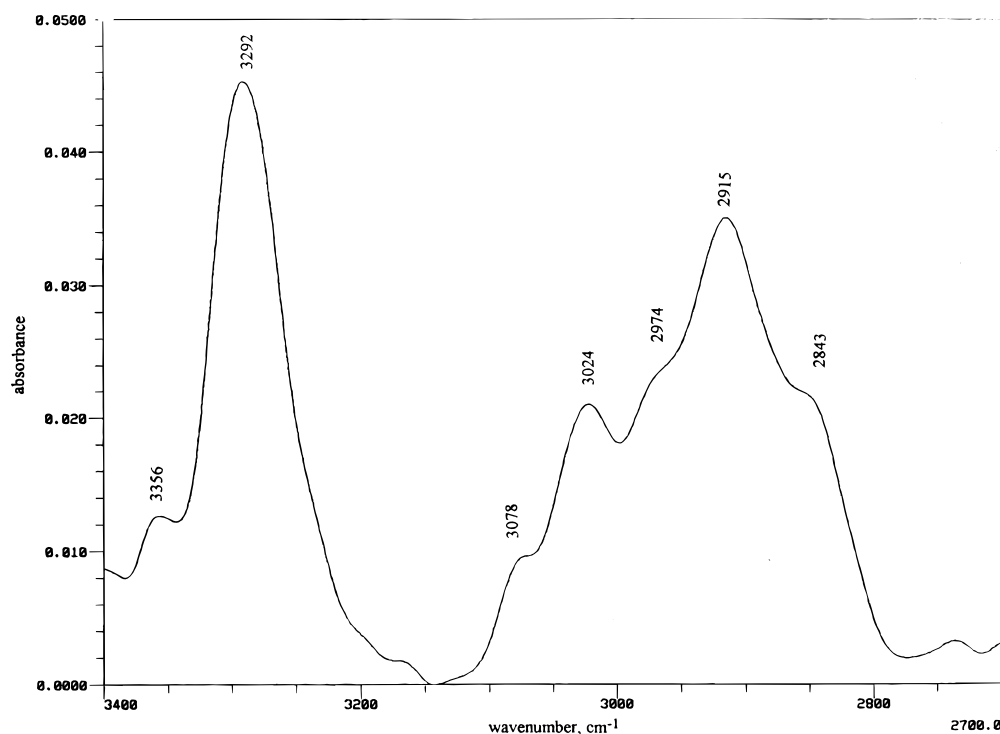


FIG. 1.—FTIR spectrum between 3400 and 2700 cm^{-1} showing C—H stretching absorption features of LT 9 MeV α -particle-irradiated C_2H_2 targets

benzenes at 1030, 1028, 1026, 835, and 793 cm^{-1} . FTIR spectra of LT and HT irradiated deuterated samples, however, failed to identify any aromatic species except benzene.

In contrast to hydrocarbon systems with larger H/C contents of 4:1 (CH_4) and 2:1 (C_2H_4), only C_2H_2 experiments supply solid residues after annealing irradiated targets to 293 K. Figure 1 displays a typical FTIR spectrum of a yellow up to red solid residue in the 3700–3400 cm^{-1} region of C≡H stretching vibrations: 3356 and 3292 cm^{-1} bands characterize acetylenic ($\equiv\text{C}-\text{H}$), and 3078 cm^{-1} absorption olefinic CH_2 groups, whereas features at 3024, 1005.5, 1023, 978, 961.6, 940, and 919.3 cm^{-1} verify complex PAHs with isolated H atoms; see Table 3. The 1005.5 and 1023 cm^{-1} bands are characteristic for PAHs such as chrysene, perylene, pentacene, and coronene; see Figure 2. The δ_{op} and δ_{ip} absorptions at 1365, 1280, 1265, 1233, 1093, 1081, 1036, 1004, 997, 975, 929, and 756 cm^{-1} in bombarded C_2H_2 systems underline the existence of di-, tri-, and tetra-substituted benzenes, enhanced approximately threefold as compared to each α -particle irradiation of CH_4 . The absorption at 855 cm^{-1} is well characterized as C—H deformation modes of isolated hydrogen atoms in naphtha-

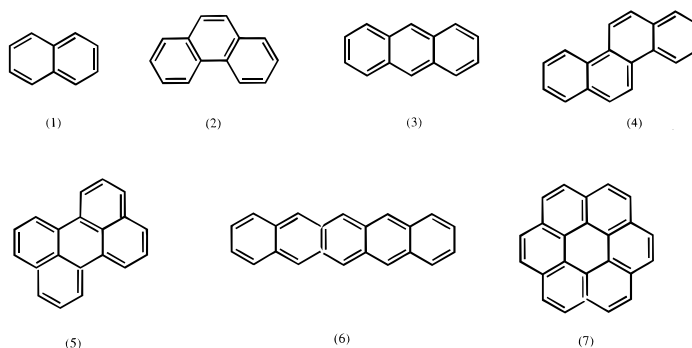


FIG. 2.—Detected PAHs in CH_4 [naphthalene (1), phenanthrene (2), anthracene (3)] and C_2H_2 irradiated targets [chrysene (4), perylene (5), pentacene (6), coronene (7)].

lene molecules. Finally, methyl and aliphatic methylene groups absorptions are shown at 2974, 2915, and 2843 cm^{-1} . These findings are in strong contrast to, e.g., Strazzulla (1985) supplying stable residues even after CH_4 -target irradiation at lower doses than applied in our experi-

TABLE 3
IR ABSORPTION FEATURES OF AROMATIC SPECIES AND ASSIGNMENTS AFTER 9 MeV α -PARTICLE IRRADIATION OF C_2H_2 AT 10 K

Absorption (cm^{-1})	Assignment
3024	Aromatic CH-stretching vibration
1005.5, 1023	Deformation modes of chrysene and/or perylene, pentacene, coronene, benzo[a]-perylene
1365, 1280, 1265, 1233, 1093, 1081, 1036, 1004, 997, 975, 929, 756	In-plane and out-of-plane deformation modes of di-, tri-, and tetra-substituted benzenes
855	C—H deformation mode of isolated H atoms in naphthalene

TABLE 4
PRODUCTION RATIOS MEASURED BY MASS SPECTROMETRY OF
SYNTHESIZED AROMATIC MOLECULES

Species	n_p, α^a	$n\alpha, \text{CH}_4/\text{C}_2\text{H}_2^b$	$n\alpha, \text{CH}_4/\text{C}_2\text{H}_4^c$
C_6H_6	(0.02 ± 0.008)	(0.15 ± 0.05)	(1 ± 0.3)
C_{10}H_8	0	(0.15 ± 0.05)	(0.25 ± 0.05)
$\text{C}_{14}\text{H}_{10}$	0	(1.4 ± 0.6)	(0.5 ± 0.2)

^a Ratio of number of molecules in LT 9 MeV α -particle irradiation of $^{12}\text{CH}_4$ to LT 7.3 MeV proton irradiation of $^{12}\text{CH}_4$.

^b Ratio of number of molecules in LT 9 MeV α -particle irradiation of CH_4 to C_2H_2 .

^c Ratio of number of molecules in LT 9 MeV α -particle irradiation of CH_4 to C_2H_4 .

ments. Differences in our results are based predominantly on contamination effects of molecular oxygen in previous experiments, as discussed in Kaiser et al. (1995b).

4.1.3.2 Quadrupole Mass Spectrometry

In strong contrast to proton experiments, 9 MeV α -particle bombardments of $^{12}\text{CH}_4$ and $^{13}\text{CH}_4$ form naphthalene/azulene and phenanthrene/anthracene molecules. Further, experiments reveal a strong temperature dependence of their yields: HT results show an increase by a factor of 5 ± 2 for benzene, by 10 ± 4 for naphthalene/azulene, and by 10 ± 2 for phenanthrene/anthracene as compared to 10 K irradiation (Table 4). In addition, the naphthalene/azulene yield increases steeply up to a factor of 7 when the H/C ratio is reduced from 4:1 ($^{12}\text{CH}_4$) over 2:1 (C_2H_4) to unity (C_2H_2). Data analysis via matrix interval algebra quantifies the total PAH yield during LT 9 MeV α -particle irradiation to $0.5\text{--}6.1 \times 10^{12}$ PAH molecules (Kaiser et al. 1995b).

Likewise, the QMS data confirm the FTIR analyses of irradiated CD_4 samples and show no fragmentation patterns of perdeuterated PAHs. However, substituted (R) perdeutero benzenes ($\text{R-C}_6\text{D}_5$) were sampled by probing $m/e = 94$ (C_7D_5^+) and $m/e = 98$ (C_7D_7^+). Parent ions of perdeutero benzene C_6D_6 ($m/e = 84$), however, interfere with perdeutero pentane isomers and exclude identification. Finally, elevated temperatures of HT as compared to LT experiments increase ion currents of $\text{R-C}_6\text{D}_5$ fragments at $m/e = 98$, by a factor of 3–4.

4.2. Computer Simulations

The elastic energy transfer, LET_n , of 7.3 MeV protons and 9 MeV α particles of $4 \pm 0.5 \text{ keV } \mu\text{m}^{-1}$ and $40 \pm 3 \text{ keV } \mu\text{m}^{-1}$ ignites primary knock-on particles (PKOs; first generation of knock-on particles). The lower LET_n of system 1 ($2.5 \pm 0.1 \text{ eV } \mu\text{m}^{-1}$) to system 2 ($29 \pm 1 \text{ eV } \mu\text{m}^{-1}$) is reflected in a decrease of generated carbon and hydrogen PKOs from 27,994 to 2600 as well as lower kinetic energies of 2 keV C— and H— (system 1) as compared to 28 keV H— and 17 keV C— PKOs (system 2). Since typical C—H and C—C/C=C/C \equiv C bond strengths range between 3 and 8.5 eV, PKOs cannot form stable chemical bonds before their excess kinetic energy is released. This additional energy transfer takes place via consecutive encounters of a PKO with the target atoms and generates a collision cascade of secondary, tertiary, etc., knock-ons. Figure 3 presents the total number of C and H knock-on particles as a function of the primary C and H knock-on energy in a $5 \mu\text{m}$ CH_4 target. The averaged, total number of C and H atoms

contributing to each collision cascade increase with rising energy from, e.g., 3.2–5.7 H knock-ons (0.1 keV C PKO) to 318–332 H knock ons. Moderated to 1–10 eV C or H PKOs can react finally with the target molecules via bond insertion, addition to double or triple bonds, or hydrogen abstraction (Fig. 4). Most important, C atoms dropped from a collision cascade are not distributed homogeneously throughout the target but are rather localized; see Figures 5a–5f. The 0.1 keV H, 1 keV H, and 10 keV H PKOs trigger cascades with only one to two suprathreshold carbon atoms. The majority of the suprathreshold C and H atoms generated by 1 keV and 10 keV carbon PKOs are concentrated in volumina of $10^2\text{--}10^3 \text{ \AA}^3$ (typically four to five C atoms), and $6 \times 10^3\text{--}5 \times 10^4 \text{ \AA}^3$ (one to two subcascades, each with 10–25 suprathreshold C atoms).

5. DISCUSSION

5.1. Mechanistic Model

Since the experiments were performed under bulk conditions, no detailed information on the molecular reaction dynamics is obtained. Therefore, we cannot elucidate an exact reaction mechanism that accounts for the PAH formation, but we infer rather a model based on collision cascade simulations and the following experimental results as described in § 4:

1. LT 7.3 MeV proton irradiation of $^{12}\text{CH}_4$ yields benzenes and substituted benzenes, but no PAHs.
2. LT 9 MeV α -particle irradiation of CD_4 target synthesizes benzenes and substituted benzenes, but no perdeutero PAHs.
3. Besides benzene and substituted benzenes, LT 9 MeV α -particle irradiation of $^{13}\text{CH}_4$ and $^{12}\text{CH}_4$ form naphthalene/azulene, anthracene/phenanthrene, and mono[di(?)]substituted anthracenes/phenanthrenes. Matrix interval algebra quantifies the total PAH yield to $0.5\text{--}6.1 \times 10^{12}$ molecules.
4. LT 9 MeV α C_2H_2 irradiation results in the formation of chrysene, perylene, benzo[a]perylene, pentacene, and/or coronene.
5. Changing the C/H ratio from 1:4 (CH_4) via 1:2 (C_2H_4) to 1:1 (C_2H_2) results in an increased PAH yield in LT 9 MeV α -particle experiments by a factor of 2–10.
6. Transition from LT to HT 9 MeV α -particle irradiation increases naphthalene/azulene and phenanthrene/anthracene yields by 1 order of magnitude.

Most striking, protons initiate carbon PKOs with kinetic energies up to 1 keV in methane frosts, whereas carbon PKOs released by α -particles hold up 17 keV. This enlargement goes hand in hand with an enhanced elastic energy transfer as quoted above. Since proton bombardments of CH_4 do not yield PAH molecules (result 1), but PAHs were detected in α -particle-irradiated systems (result 3), their formation should correlate with the elastic linear energy transfer. LET_n data in our as well as earlier experiments support strongly this conclusion, and PAHs could be sampled only in systems with $\text{LET}_n > 2.5 \pm 0.2 \text{ eV } \mu\text{m}^{-1}$; see Table 5 (Patnaik, Roessler, & Zador 1990; Kaiser & Roessler 1992).

Since the nuclear linear energy transfer relates to the total number of suprathreshold C and H atoms as found in § 4.2 and PAH molecules can be formed solely in the energized volumina within single-collision cascades, the spatial distribution of reactive C and H atoms is of fundamental

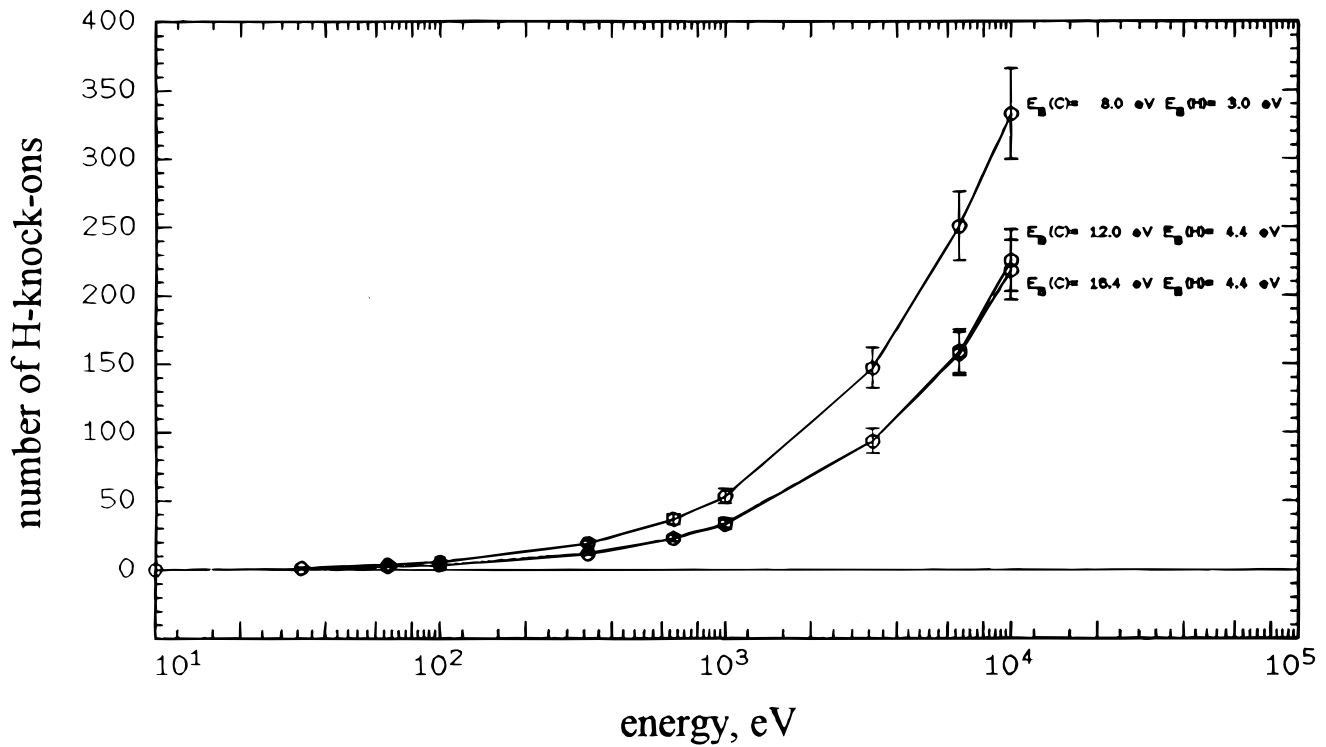


FIG. 3a

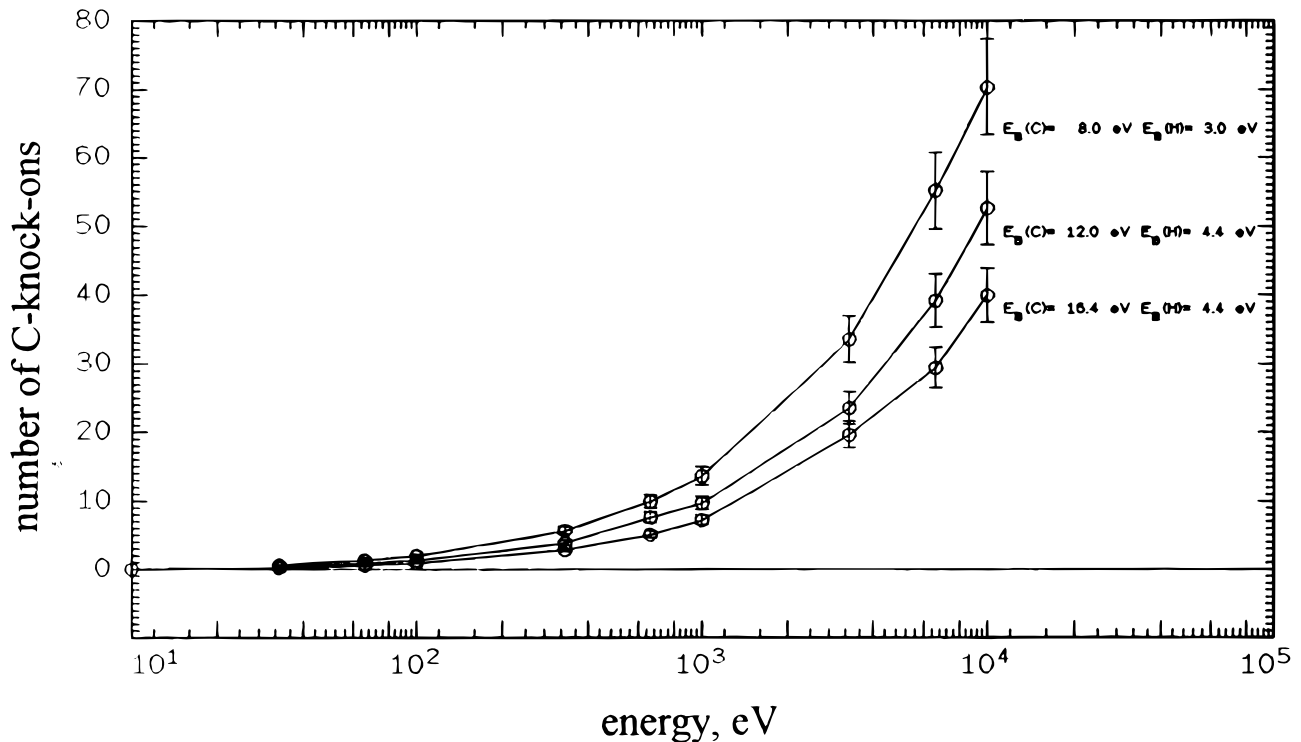


FIG. 3b

FIG. 3.—Total number of hydrogen and carbon knock-on particles as a function of carbon and hydrogen PKO particle energy. Three sets of displacement energies are calculated, i.e., $E_B(C) = 16.4 \text{ eV}/E_B(H) = 4.4 \text{ eV}$, $E_B(C) = 12.4 \text{ eV}/E_B(H) = 4.4 \text{ eV}$, and $E_B(C) = 8 \text{ eV}/E_B(H) = 3 \text{ eV}$. (a) C PKO, H knock-ons; (b) C-PKO, C knock-ons; (c) H PKO, H knock-ons; (d) H PKO, C knock-ons.

importance. Overlapping cascades can be ruled out because even doses as low as 10^{-3} eV —much smaller than the threshold to the overlap regime—produce PAHs (Roessler 1992). Both conclusions impose an upper limit of the PAH dimensions to 4–10 Å (system 1) and 18–22 Å (system 2); see

Figures 5a–5f and § 4.2. If we compare these magnitudes with the maximum distance of two hydrogen atoms in detected PAHs naphthalene ($\approx 8 \text{ Å}$), phenanthrene ($\approx 10 \text{ Å}$), anthracene ($\approx 10 \text{ Å}$), pyrene ($\approx 10 \text{ Å}$), and coronene ($\approx 10 \text{ Å}$), naphthalene should be found in proton (system 1)

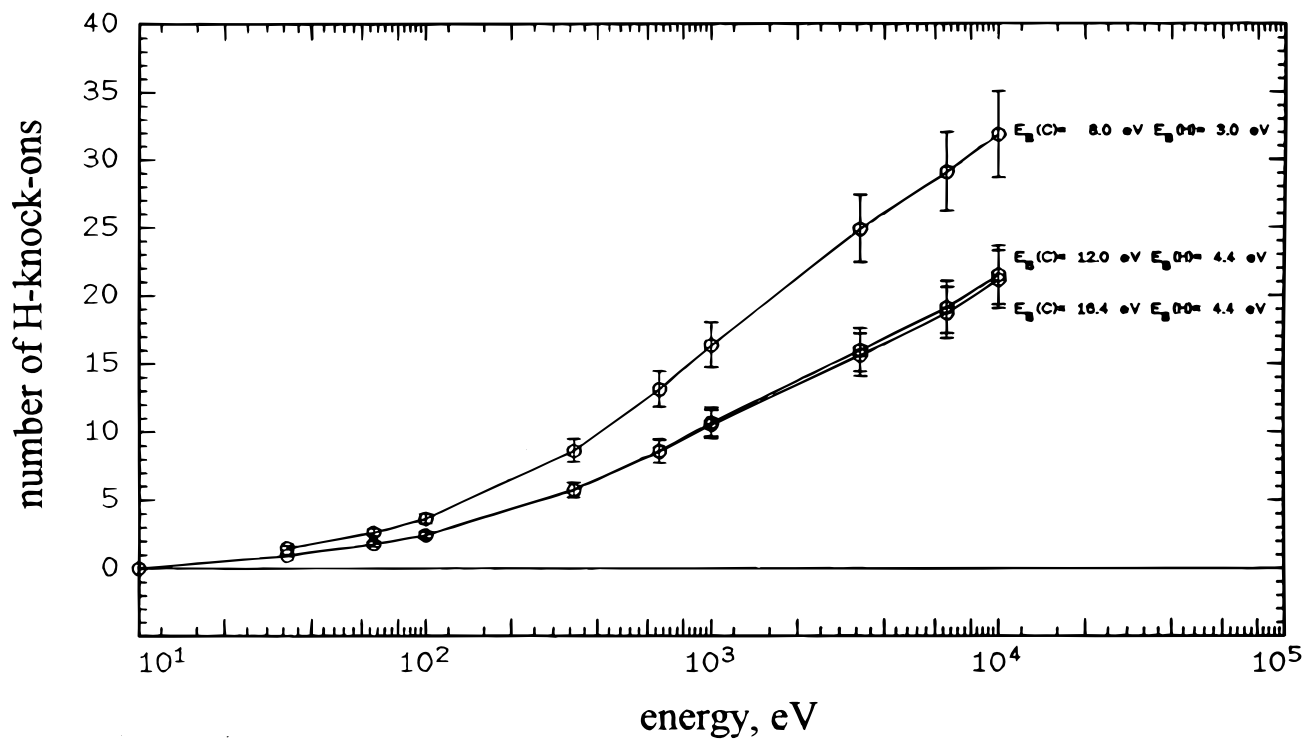


FIG. 3c

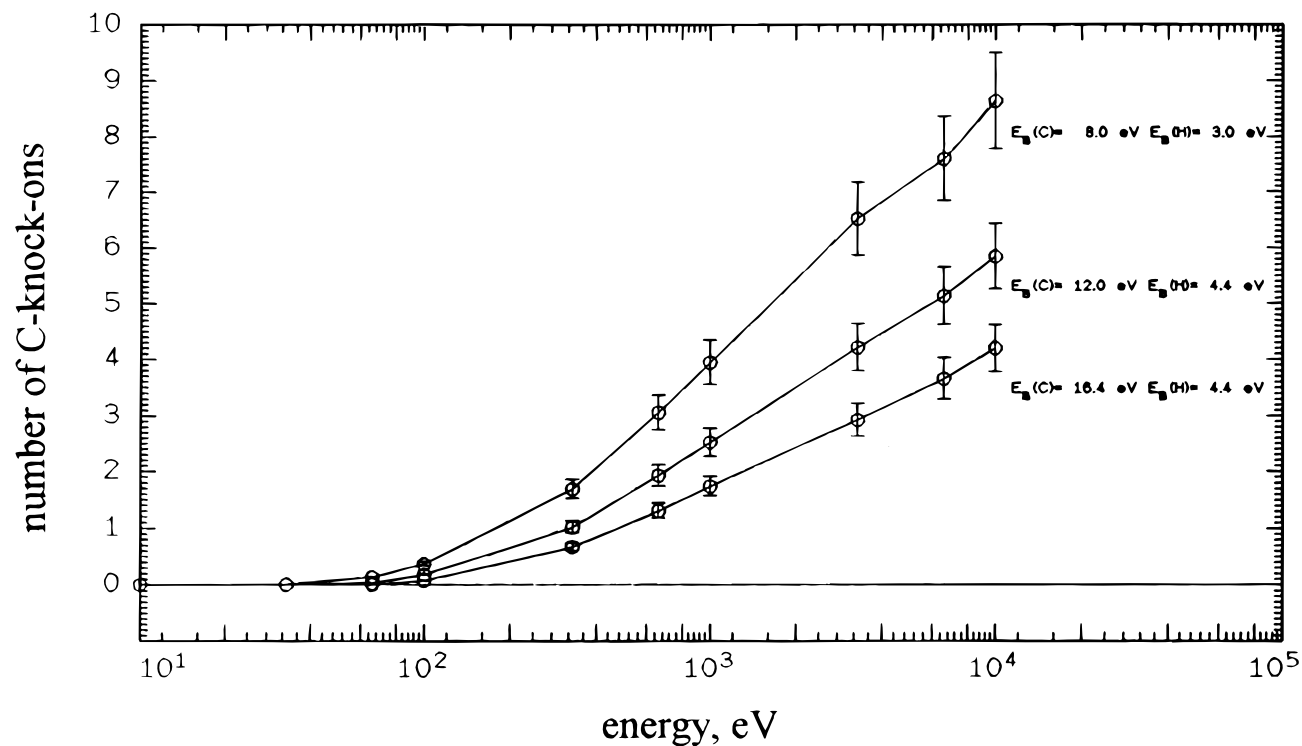


FIG. 3d

as well as α -particle-irradiated targets (system 2). Phenanthrene, anthracene, and coronene range only at the upper limit of system 1 found in one of 10^4 calculated collision cascades and should dominate in system 2. Adopting average yields of C PKOs in 9 MeV α irradiation (§ 4.2) and integrating over the irradiation time with the ion flux and

ion beam area (Table 1), a maximum number of $2.5 \pm 1.2 \times 10^{12}$ PAH molecules can be formed. This value agrees strongly with result 3.

Despite the fulfillment of the geometrical requirement, the largest accessible PAH molecules naphthalene and coronene were not synthesized in system 1 and 2, respec-

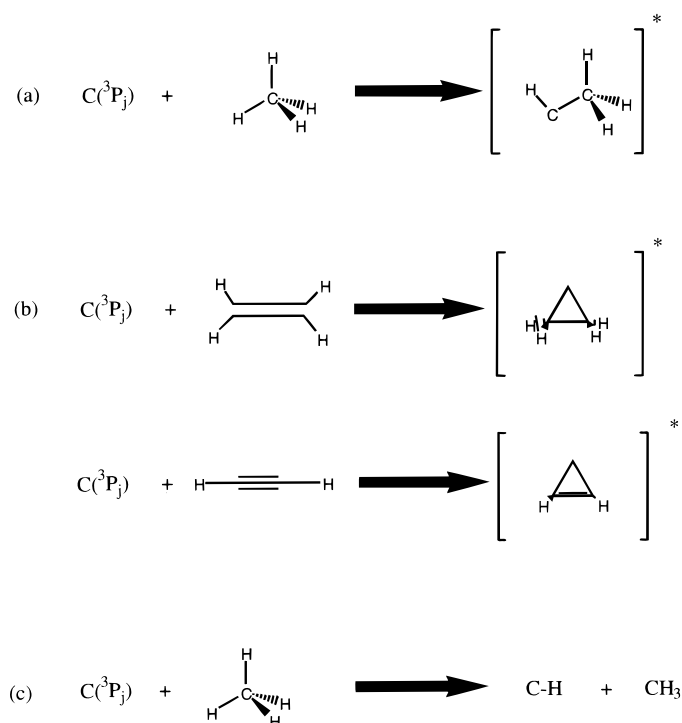


FIG. 4.—Elementary reactions of suprathermal carbon atoms in its electronic 3P_j ground state. (a) Insertion in a C—H bond of methane to a triplet methylcarbene; (b) addition to double or triple bonds forming triplet cyclopropylidene or cyclopropenylidene; (c) hydrogen abstraction to CH and CH_3 radicals.

tively. What inhibits the formation? As stated above, each PAH is generated within a single-collision cascade comprising suprathermal H and C atoms. Every carbon atom forms an individual reaction center of abstraction, insertion, and addition at the end point of its trajectories. In the relaxation phase of this energized volume, overlapping reaction zones of single reaction centers may synthesize complex molecules such as the detected PAHs. Hereafter, we denote this model “multicenter mechanism.”

In terms of this model, the product of a multicenter mechanism depends strongly on the local C/H ratio: a carbon-enriched target yields an enhanced number of newly formed carbon-carbon bonds as compared to carbon-hydrogen ones in the relaxation phase. Therefore, a reaction product with a higher C/H ratio is expected. This conclusion matches our experimental findings 2 and 4–6. The temperature increase from 10 to 50 K results in a 30,000-fold enlargement of H_2 formation and a reduction of the H/C ratio in the energized volumina during a HT CH_4 irradiation

as compared to the LT experiment (see § 4) and contributes to a higher naphthalene yield (result 6) as the H-diffusion coefficient rises. Likewise, a reduced C/H reactant ratio from 1:1 (C_2H_2) to 1:4 (CH_4) increases the total PAH yield (result 4) and forms complex PAHs only in irradiated targets with an initial, macroscopic high carbon content (result 5). Following this argument, the inhibited naphthalene (system 1) and coronene synthesis (system 2) are a result of a microscopic insufficient carbon enrichment to form molecules with C/H ratios of 1.25 (naphthalene) and 2.0 (coronene) in environments with an initial C/H ratio of 0.25. This effect was observed in preliminary studies of PAH formation in experiments by Patnaik et al. (1978) and Kaiser & Roessler (1992): 20 MeV $^3\text{He}^{2+}$ CH_4 bombardment at 77–85 K generates PAHs up to coronene, whereas 17 MeV $^3\text{He}^{2+}$ experiments at 30–50 K are restricted to lower mass PAHs up to pyrene. Finally, our model gains support from CD_4 irradiated systems with no perdeutero PAHs, which can be explained in terms of a reduced diffusion coefficient of D compared to H at a constant temperature and, hence, a lower local carbon content in the deuterated sample correlating with the inhibited PAH formation (result 2).

5.2. Alternative Irradiation Experiments

Our model emphasizes the crucial role of *suprathermal carbon atoms* and *collision cascades* to form PAH molecules. In this section, we test this model against alternative radiation exposures of the CH_4 target. If our multicenter reaction holds, any experimental condition that cannot fulfill one of the highlighted requirements should not yield PAH species.

UV photolysis and radiolysis of hydrocarbon targets at 20–77 K support the multicenter nature of our model: vacuum UV photons interact in single quantum processes with a CH_4 molecule and cannot generate collision cascades (Fig. 5). A $^{60}\text{Co}-\gamma$ quantum transfers its energy in successive collisions to the target, but no collision cascades are initiated. In strong agreement with our model, no PAHs could be detected. Finally, irradiation of gaseous methane targets shows no polycyclic aromatic hydrocarbons, since the required number density of reactive carbon atoms cannot be generated (Davis, Libby, & Menschein 1966).

6. ASTROPHYSICAL IMPLICATIONS AND CONCLUSIONS

The conceptual framework of the multicenter mechanism clarifies formation of the PAHs naphthalene, alkyl-naphthalenes, and phenanthrene in Murchison, Allende, and Orgueil chondrite as well as detected O and N substituted PAHs. Hetero PAHs are predicted to be synthesized

TABLE 5
CORRELATION OF LET_n VALUES WITH PAH SYNTHESSES

Target	Implant	Energy (MeV)	LET_n ($\text{eV } \mu\text{m}^{-1}$)	PAH Formation	Temperature (K)
$^{12}\text{CH}_4$	p	17.4	1.1 ± 0.1	No	77–85
	p	17.6	1.1 ± 0.1	No	< 50
	p	7.3	2.5 ± 0.2	No ^a	10–15
	$^3\text{He}^{2+}$	16	13.1 ± 0.5	Yes	77–85
	$^3\text{He}^{2+}$	7.3	26.3 ± 0.5	Yes	< 30
$^{13}\text{CH}_4$	α	9	28.9 ± 0.6	Yes ^a	10–15
	α	9	29.0 ± 0.8	Yes ^a	10–15

^a Present experiments.

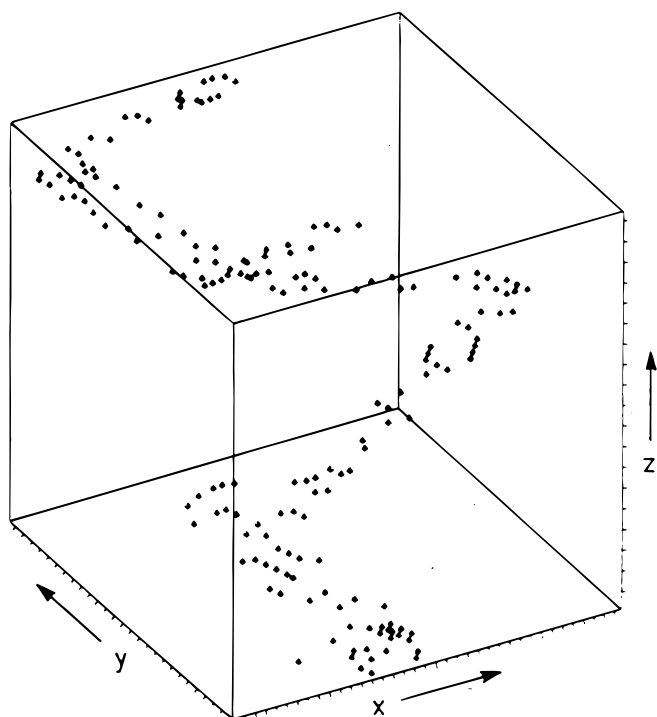


FIG. 5a

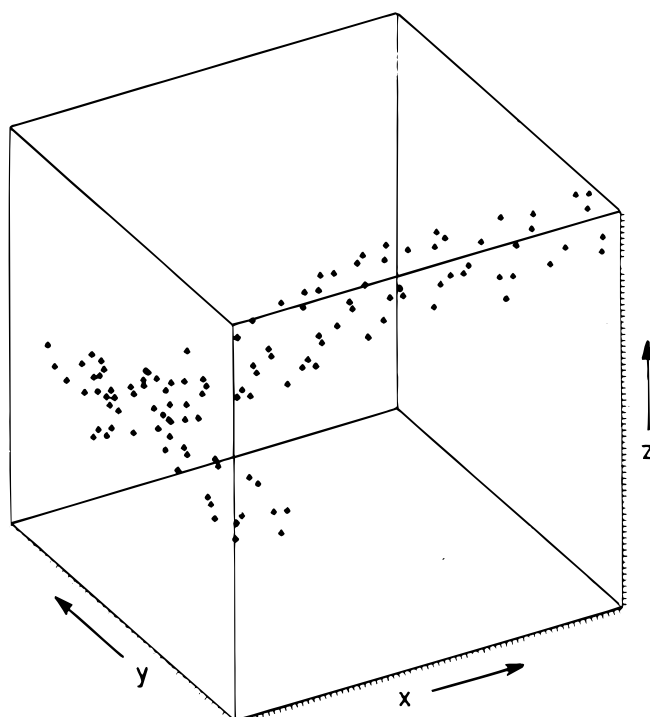


FIG. 5b

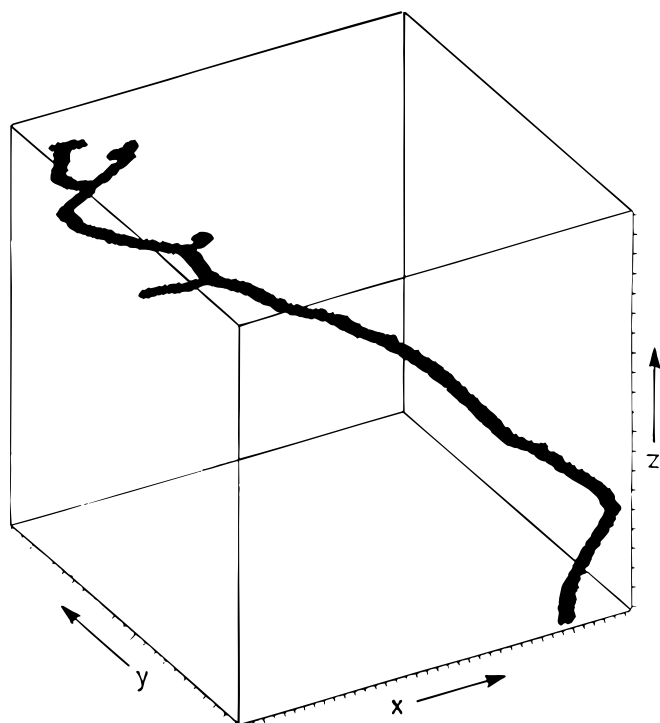


FIG. 5c

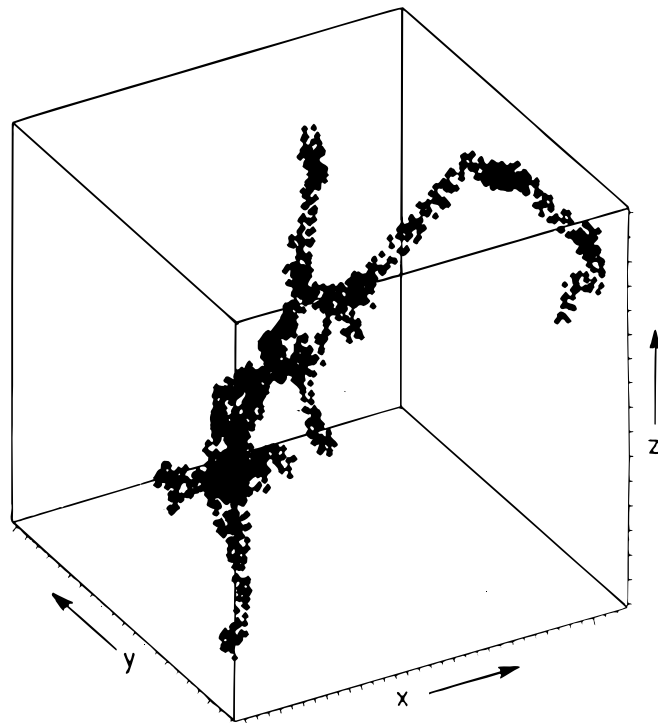


FIG. 5d

FIG. 5.—Three-dimensional plots of C and H PKO initiated collision cascades for 0.1, 1, and 10 keV PKO energy and a displacement energy set $E_D(\text{C}) = 12.4$ eV and $E_D(\text{H}) = 4.4$ eV, respectively. Each dot represents an inelastic encounter with a target atom, whereas large concentrations of dropped hydrogen and carbon atoms are indicated by arrows. The x, y, and z dimensions are given in units of angstroms as (a) $x = 5$, $y = 24$, $z = 30$ (0.1 keV H PKO); (b) $x = 18$, $y = 12$, $z = 18$ (0.1 keV C PKO); (c) $x = 54$, $y = 150$, $z = 300$ (1 keV H PKO); (d) $x = 90$, $y = 60$, $z = 45$ (1 keV C PKO); (e) $x = 450$, $y = 600$, $z = 2700$ (10 keV H PKO); and (f) $x = 250$, $y = 860$, $z = 650$ (10 keV C PKO).

in extraterrestrial ice mixtures containing predominantly CH_4 , NH_3 , H_2O , CO , and CH_3OH by inclusion of N/O knock-on atoms and N/O containing molecules in the relaxation phase of the energized volumina. In analogy to our hydrocarbon model compounds, astrophysical relevant

ice mixtures require critical H/C, C/O, and C/N ratios. Otherwise, insertion, addition, and abstraction processes as well as the statistical combination of a multiplicity of reaction centers cannot build up carbon skeletons large enough to synthesize hetero PAHs.

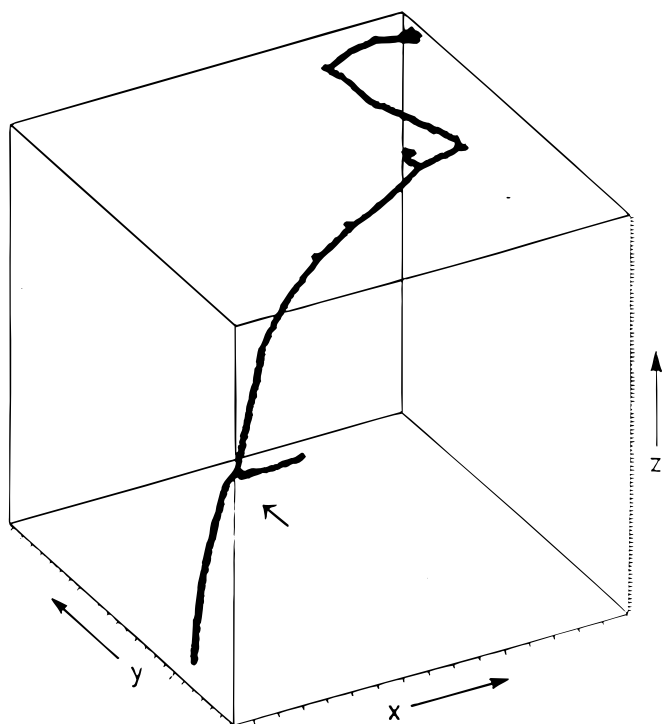


FIG. 5e

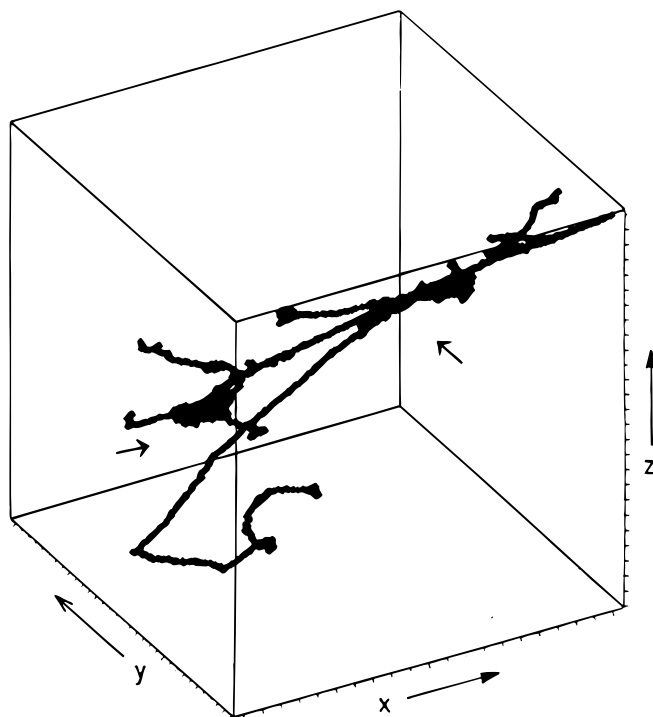
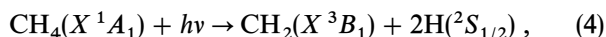
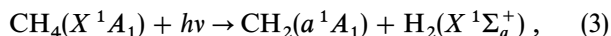


FIG. 5f

FIG. 5.—Continued

Since only 1%–8% of interstellar grain material condenses as CH₄, either high carbon concentrations or enrichment processes donate the required carbon density. The reactivity preference of suprathermal knock-on particles in interstellar ices support this conclusion: suprathermal H atoms prefer to abstract hydrogen atoms and react to H₂, N and O atoms favor N₂ and O₂ formation, respectively, whereas suprathermal C particles tend to generate CO and carbon-carbon bonds; see Table 6 (Roessler 1992). In addition, the cosmic UV radiation field ($\phi = 4 \times 10^3 \text{ cm}^{-2} \text{ s}^{-1}$) supports hydrogen elimination by photolyzing, e.g., CH₄:



to reduce the hydrogen content after H recombination to H₂, diffusion to the grain surface, and desorption into gas phase. These synergistic effects of simultaneous MeV α -photon irradiation of CH₄ should lead to an enhanced PAH production.

In our solar system, PAH formation can be induced by direct implantation of keV ions into CH₄ targets. Although the contribution of keV particles in the galactic cosmic-ray

is marginal, the solar radiation field with a flux of $\phi = 2\text{--}3 \times 10^8 \text{ cm}^{-2} \text{ s}^{-1}$ (at 1 AU; AU = distance between Earth and Sun) peaks at energies of $\approx 1 \text{ keV amu}^{-1}$. The solid CH₄ distribution is well documented on Triton, Uranus, Neptune, and Pluto and its moon Charon; hence, PAH formation might take place. In addition, UV photons and keV particles penetrate only the very first 0.2–0.5 μm of the ice layers, whereas projected ranges of MeV particles extent to 10^{-3} m inside the target. Consequently, a chemical differentiation occurs in hydrocarbon-rich ices: hydrogen-depleted outer zones (keV particles and UV radiation) versus hydrogen-rich, inner regions of planetary surfaces.

Simulation experiments of the interaction of galactic cosmic-ray particles with frozen matter in space can never simulate the complexity of interstellar environments, e.g., a wide energy range as well as chemical composition of the cosmic rays, UV irradiation field, and composition of ice targets itself. Understanding of these processes *must* be based on simulation experiments involving relatively simple *model systems* under controlled circumstances before extending experiments to more complex systems. Further, simulation experiments accelerate natural processes: 1 s of our MeV irradiation simulates $3 \times 10^{10} \text{ s}$ in space. Long-term effects such as tunneling processes in interstellar ices are hard to elucidate. The derived multicenter mechanism, however, resembles a versatile synthetic route to complex molecules within single-collision cascades and is transferable without any restrictions to extraterrestrial ices or amorphous carbon grains (Snow et al. 1995).

TABLE 6

REACTIVITY PREFERENCE OF SUPRATHERMAL PARTICLES WITH ICE TARGETS CONTAINING C, O, N, AND H

Suprathermal Particle	Reactivity Preference
H	H > N > O > C
C	O \approx C > H \gg N
N	N \geq H \approx O > C
O	O > C \approx H \gg N

The authors want to thank the cyclotron crew of the compact cyclotron CV 28 at the Forschungszentrum Jülich for performing the irradiation and Professor G. Stöcklin, director of Institut für Nuklearchemie, for his invaluable

assistance with financing the experimental setup. One of us (R. I. K.) is indebted to the Deutsche Forschungsgemeinschaft (DFG) for financial support to present parts of the present work on Radiation-Effects in Insulators (REI-7, Nagoya, Japan) and to Professor B. Krebs, Westfälische

Wilhelms Universität Münster, for administrative guidance and advice. We are grateful to W. Schutte, University of Leiden, The Netherlands, for careful reading of and comments on an earlier version of the manuscript.

REFERENCES

- Allain, A., Leach, S., & Sedlmayr, S. 1996a, *A&A*, 305, 602
 ———. 1996a, *A&A*, 305, 616
 Allamandola, L. J. 1990, in *Topics in Current Chemistry*, ed. S. Cyvin, & J. Gutman (Berlin: Springer), 1
 Allamandola, L. J., Sandford, S. A., & Wopenka, B. 1987, *Science*, 237, 56
 Allamandola, L. J., Tielens, A. G. G. M., & Barker, J. R. 1985, *ApJ*, 290, L25
 Bakes, E. L. O., & Tielens, A. G. G. M. 1994, *ApJ*, 427, 822
 Bergman, J., Larson, K., Rank, D., & Termi, P. 1994, *ApJ*, 423, 326
 Davis, D. R., Libby, W. F., & Menschein, W. G. 1966, *J. Chem. Phys.*, 45, 4481
 Duley, W. W. 1994, *ApJ*, 429, L91
 Eckstein, W. 1991, *Computer Simulation of Ion-Solid Interaction* (Berlin: Springer)
 Ehrenfreund, P., Foing, B. H., d'Hendecourt, L., Jenniskens, P., & Desert, F. X. 1995, *A&A*, 299, 213
 Encrenaz, T., d'Hendecourt, L., & Puget, J. L. 1988, *A&A*, 207, 162
 Firsov, O. B. 1957, *Soviet Phys.—JETP*, 5, 1192
 ———. 1962, *Soviet Phys.—JETP*, 36, 1076
 Frenklach, M., & Feigelson, E. D. 1989, *ApJ*, 341, 372
 Geballe, T. R., Tielens, A. G. G. M., Allamandola, L. J., Moorehouse, A., & Brand, P. W. J. L. 1989, *ApJ*, 341, 278
 Hagen, W. 1987, Ph.D thesis, Univ. Leiden
 Hayatsu, R., Matsuoka, S., Scott, R. G., Studier, M. H., & Anders, E. 1979, *Geochim. Cosmochim. Acta*, 41, 1325
 Joblin, C., Boissel, P., Leger, A., d'Hendecourt, L., & Defourneau, D. 1995, *A&A*, 299, 835
 Joblin, C., d'Hendecourt, L., Leger, A., & Defourneau, D. 1994, *A&A*, 281, 923
 Joblin, C., Tielens, A. G. G. M., Geballe, T. R., & Wooden, D. H. 1996, *ApJ*, 460, L119
 Jochims, H. W., Rühl, E., Baumgärtel, H., Tobita, S., & Leach, S. 1994, *ApJ*, 420, 307
 Kaiser, R. I., Gabrysch, A., & Roessler, K. 1995a, *Rev. Sci. Instrum.*, 66, 3058
 Kaiser, R. I., Jansen, P., Petersen, K., & Roessler, K. 1995b, *Rev. Sci. Instrum.*, 66, 5226
 Kaiser, R. I., & Roessler, K. 1992, *Ann. Geophys.*, 10, 222
 Langhoff, S. R. 1996, *J. Phys. Chem.*, 100, 2819
 Leger, A., & Puget, J. L. 1984, *A&A*, 137, L5
 Millar, T. J., Roueff, E., Charnley, S. B., & Rodgers, S. D. 1995, *Int. J. Mass Spectrom. Ion Processes*, 149/150, 389
 Molière, G. Z. 1947, *Z. Naturforsch.*, A2, 133
 Mullie, F., & Reisse, J. 1987, in *Topics in Current Chemistry* (Berlin: Springer), 83
 Patnaik, A., Roessler, K., & Zador, E. 1990, in *Lun. Planet. Sci. Conf. XXI*, 1035
 Pauzat, F., Talbi, D., & Ellinger, Y. 1995, *A&A*, 293, 263
 Pearl J. 1994, private communication
 Robinson, M. T. 1992, *Nucl. Instrum. Methods*, B67, 396
 Roessler, K. 1992, in *Handbook of Hot Atom Chemistry* (Tokyo/Weinheim: Kodansha/VCH), 265
 Salama, F., & Allamandola, L. J. 1991, *J. Chem. Phys.*, 94, 6964
 ———. 1992, *ApJ*, 395, 301
 Salama, F., Joblin, C., & Allamandola, L. J. J. 1994, *J. Chem. Phys.*, 101, 10252
 Schutte, W. A., Tielens, A. G. G. M., & Allamandola, L. J. 1993, *ApJ*, 415, 397
 Schutte, W. A., Tielens, A. G. G. M., Allamandola, L. J., Cohen, M., & Wooden, D. H. 1990, *ApJ*, 360, 577
 Siebenmorgen, R., & Peletier, R. F. 1994, *A&A*, 279, L45
 Smit, W. M. A., van Straten, A. J., & Visser, T. 1978, *J. Mol. Struct.*, 48, 177
 Snow, T. P., Bakes, E. L. O., Russ, R. H., & Seab, C. G. 1995, *A&A*, 296, L37
 Stein, S. E. 1978, *J. Chem. Phys.*, 82, 566
 Stöcklin, G. 1969, *Chemie heißer Atome* (Weinheim: VCH)
 Strazzulla, G. 1985, *Icarus*, 61, 48
 Trakhtenberg, L. I., Milikh, G. M. 1983, *Khimiya Vysokikh Energii*, 17, 483